MESOSCALE DIAGNOSTIC QUANTITIES FROM ARRAYS OF DOPPLER WIND PROFILERS AND RADIOSONDES

Gerald G. Mace, Thomas P. Ackerman and Eugene Clothiaux
The Pennsylvania State University
University Park, PA.

1. INTRODUCTION

It has been recognized for some time that clouds are one of the most important yet least understood modulators of the global climate system. In order to increase understanding of the coupling of the cloud scale processes with the larger scale environment, ambitious field programs have recently been conducted. An example of this effort is represented by the First International Satellite Cloud Climatology Project (ISCCP) Regional Experiment (FIRE Cirrus II). This intensive field campaign was conducted in Coffeyville, Kansas in November and December, 1991. These types of field campaigns are useful in the sense that highly detailed process studies can be undertaken. These process studies ultimately increase our understanding of the coupling of the cloud scale dynamical and radiative processes with the larger scale circulation in given situations.

The process studies which result from intensive field programs tend to concentrate on space and time scales well below the resolution of GCMs. While this is very useful, the parameterization problem, due to the time and space averaging in a GCM, is not completely deterministic. Given the state of the GCM resolvable variables, it must be determined if the presence of clouds is probable within the grid-box and then to determine the form the cloud forcing will take. Intensive field programs such as FIRE Cirrus II, which provide two or three good case studies, do not generate a sufficient statistical database. Creating the needed long term database will be addressed by the Atmospheric Radiation Measurement Program (ARM) which is conducting observational programs at climatically significant locations around the world. The lessons learned from intensive field campaigns such as FIRE can then be applied to the less detailed but continuous time series of data provided by ARM.

The first ARM Clouds And Radiation Testbed (CART) site is now operational near Lamont, Oklahoma. The Southern Great Plains (SGP) CART site is uniquely positioned to examine the coupling of the radiative forcing of the atmosphere with the meso and larger scale atmospheric state. This is due, in large part, to the presence of several NOAA 404 Mhz Doppler wind profilers surrounding the central observational facility (Fig. 1). These wind profilers roughly form a 200 kilometer (km) grid box around the central facility and provide wind information from 750 meters above ground level to 16 km with 250 meter vertical resolution. With the addition of thermodynamic information provided ether by radiosondes or Radio Acoustic Sounding Systems (RASS), the mesoscale atmospheric state can be nearly completely described.

This paper will present methods which combine wind profiler network observations with radiosonde measurements to create large scale variables which can be used as input to single column models, for verification of mesoscale models or for creation of a long term diagnostic data base. Results from these methods will be used in an analysis of a mesoscale cloud band observed during FIRE Cirrus II.

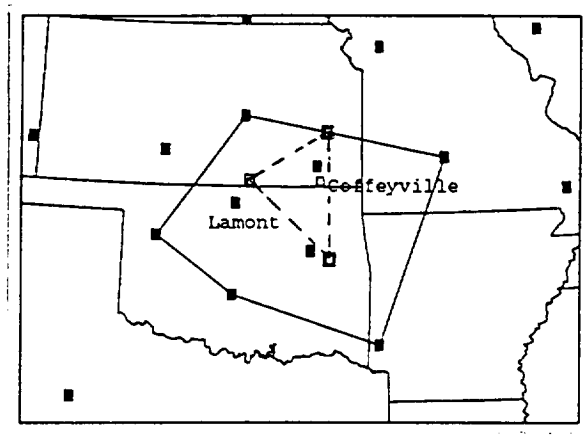

Fig. 1. Map of wind profiler locations (solid squares) and FIRE Cirrus II CLASS radiosonde sites (open squares). Solid lines connect the profiler geometry used in the analysis and dashed lines form the CLASS radiosonde triangle.

2. METHOD

2.1 Wind Profiler Polygon

Until the Wind Profiler Demonstration Array became operational, the largest array of wind profilers used in any type of diagnostic analysis consisted of three radars. As pointed out by Zamora et al (1987), the weakness of using three profilers to perform kinematic calculations is that only the linear portion of the atmospheric flow can be examined. Since atmospheric fields seldom vary in a truly linear fashion we have taken advantage of the number of wind profilers near the SGP CART site to extend the ideas of the LVPF to its next logical step.

A complete derivation of this method is presented in Mace et al (1992) and will only be summarized here. We begin by expanding a second order Taylor series for a two dimensional scalar function, α, about an arbitrary point, (x_0,y_0):

$$\alpha(x_i, y_i) = \alpha(x_0, y_0) + \frac{\partial\alpha}{\partial x}\delta x_i + \frac{\partial\alpha}{\partial y}\delta y_i + \frac{\partial^2\alpha}{\partial x^2}\frac{\delta x_i^2}{2} + \frac{\partial^2\alpha}{\partial x\partial y}\delta x_i\delta y_i + \frac{\partial^2\alpha}{\partial y^2}\frac{\delta y_i^2}{2} \quad (1)$$

where $\delta x_i=(x_i - x_0)$, $\delta y_i=(y_i - y_0)$, and the subscript i denotes an observational point. With six unknowns on the right hand side of equation 1, six independent observations of α are needed (i.e. $\alpha(x_1, y_1)$, $\alpha(x_2, y_2)$,..., $\alpha(x_6, y_6)$) to form a system of six equations with six unknowns. This system can then be solved for the spatial characteristics of α by using the geometry of the observational array to form a right hand side constant matrix. This formulation differs from the classic line integral method since a quadratic surface of the variable α is being fitted to the observations. With this quadratic fit, the zeroth and first order characteristics of the α surface can be determined anywhere within the observational array and do not represent area averaged quantities. Symmetry arguments can show that this method is robust for any non-symmetrical orientation of observations. As the observational array approaches any type of symmetry, a rectangle or hexagon for instance, the matrix composing the distance quantities approaches singularity. It turns out that the geometrical orientation of the six NOAA wind profilers which compose the SGP grid box (fig. 1) are too close to symmetrical and this method is not robust when applied to them.

This problem can be overcome by specifying the central observation, $\alpha(x_0,y_0)$, as a quantity observed by the Lamont profiler. Equation 1 can be rewritten,

$$\alpha(x_i, y_i) - \alpha(x_L, y_L) = \frac{\partial\alpha}{\partial x}\delta x_i + \frac{\partial\alpha}{\partial y}\delta y_i + \frac{\partial^2\alpha}{\partial x^2}\frac{\delta x_i^2}{2} + \frac{\partial^2\alpha}{\partial x\partial y}\delta x_i\delta y_i + \frac{\partial^2\alpha}{\partial y^2}\frac{\delta y_i^2}{2} \quad (2)$$

Where $\alpha(x_L, y_L)$ now denotes a quantity observed at the Lamont profiler location which is assumed to be known and $\delta x_i=(x_i - x_L)$, $\delta y_i=(y_i - y_L)$. With five surrounding observations, a five-equation linear system can be solved for the differential characteristics of α at the Lamont location. The method represented by (2) differs from that of (1) in that the symmetry of the profiler geometry is broken and the fit of the quadratic surface to the observations is constrained by the central observation at Lamont.

Solving this system of equations successively for the observed orthogonal wind components (u, v, w) using any five of the six profilers surrounding the Lamont profiler enables a complete determination of the differential characteristics of the atmospheric flow valid at the central observational location. This solution is limited only by the horizontal resolution of the surrounding profiler network. For convenience, we have termed this method Q6.

2.2 Radiosonde Triangle

Referring again to (1), this equation can be truncated at first order and written as

$$\alpha(x_i, y_i) = \alpha(x_0, y_0) + \frac{\partial\alpha}{\partial x}\delta x_i + \frac{\partial\alpha}{\partial y}\delta y_i$$

By using the geometry of the radiosonde triangle, the three unknowns on the right hand side can be determined if three non-colinear observations exist. Since radiosonde ascents are never vertical, nor are the observations necessarily coincident in time, accurate determination of the differential properties of the observed quantities can be obtained only by taking account of the continuously changing triangle geometries in space and time. This method has been applied to the CLASS radiosonde network data collected during FIRE Cirrus II to produce the horizontal gradient terms of pressure, temperature and vapor pressure.

2.3 Synergistic Observations

While the derived profiler and radiosonde network quantities are very useful in themselves, combining the observations provides an entirely new perspective on diagnostic analysis. For instance, vertical velocities have been calculated with observational data using both the adiabatic method and the kinematic method (Holton, 1977). Each method suffers from difficulties. When high temporal resolution radiosonde launches are available, the adiabatic method suffers principally from inaccurate wind observations. The kinematic method, however, tends to amplify any small wind errors and suffers from an inability to set boundary conditions when applied to profiler observations. Combining the highly accurate profiler wind components from the profiler observations with the temperature gradient data measured by a radiosonde or RASS network overcomes the drawbacks of the adiabatic method. An accurate estimation of the mesoscale vertical velocity field can then be determined.

Additionally, water vapor gradients can be combined with the characteristics of the horizontal flow and the calculated vertical velocity to examine quantities such as the water vapor flux divergence. This quantity is determined by using a well known vector identity and can be written

$$\nabla \cdot \mathbf{V}e = \mathbf{V}_h \cdot \nabla_h e + w \frac{\partial e}{\partial z} + e(\nabla \cdot \mathbf{V}),$$

where the subscript h represents the horizontal component, e is the water vapor pressure, $\mathbf{V}$, the wind velocity and ∇, the horizontal gradient operator.

3. RESULTS

Fig. 2 shows the 18z 26 November 1991 wind field on the 330 K isentropic surface (approximately 11 km) as determined by the Mesoscale Analysis and Prediction System (MAPS) analyses (Benjamin, 1991). The Kansas-Oklahoma region resided in the base of a broad upper level trough. At this time, a mid and upper level cloud band was propagating eastward with the upper level pattern along and ahead of the region of sharply increasing wind speed which can be observed over the Oklahoma panhandle. This cloud band extended from central Texas to a surface low pressure center in central Nebraska. The leading edge of this cloud band passed over Coffeyville, Kansas, the FIRE

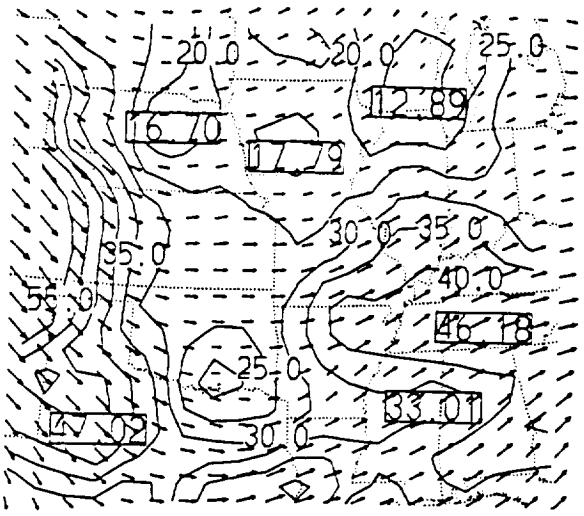

Fig. 2. Horizontal winds analyzed on the 330 Kelvin isentropic surface by MAPS. Vectors are compass direction and contours are of wind speed in m s^{-1}.

Cirrus II operational hub, at this time. Fig. 3 shows a time height cross section of reflectivities observed by the Pennsylvania State University 94 GHz cloud radar (Peters et al., 1992) which was located in Coffeyville. The leading edge of this cloud shield was first observed over Coffeyville at 8.5 km just after 1830z 26 Nov. This layer of cirrus rapidly thickened after 1900z with cloud base at 6.2 km and cloud top near 8.5 km. Cloud base shows a very gradual lowering until 2115z . This lowering was likely due to moistening of the sub-cloud air by evaporating ice crystals falling from the generating cell region above. After 2115z, a definite change in the character of the cloud was noted as cloud base lowered quite rapidly and reflectivity increased. By 2200z cloud base was observed near 3 km. Note that the radar minimum range was set at 3 km during this period, which precluded measurements below this height. Cloud base did drop below 3 km as evidenced by ceilometer measurements. Cloud top during this time was observed to decrease slightly to 8 km. The next major change in this cloud deck occurred after 2215z. Cloud top and the upper extent of the region of enhanced reflectivity became more diffuse and began to lower rapidly, while the lower portions remained nearly unchanged. By 2330z , only scattered clouds were observed by the radar.

The observed bulk structure of this cloud can be explained quite well by combining the kinematic quantities derived from the wind profilers with the radiosonde network information. The overall structure of the divergence pattern ahead of

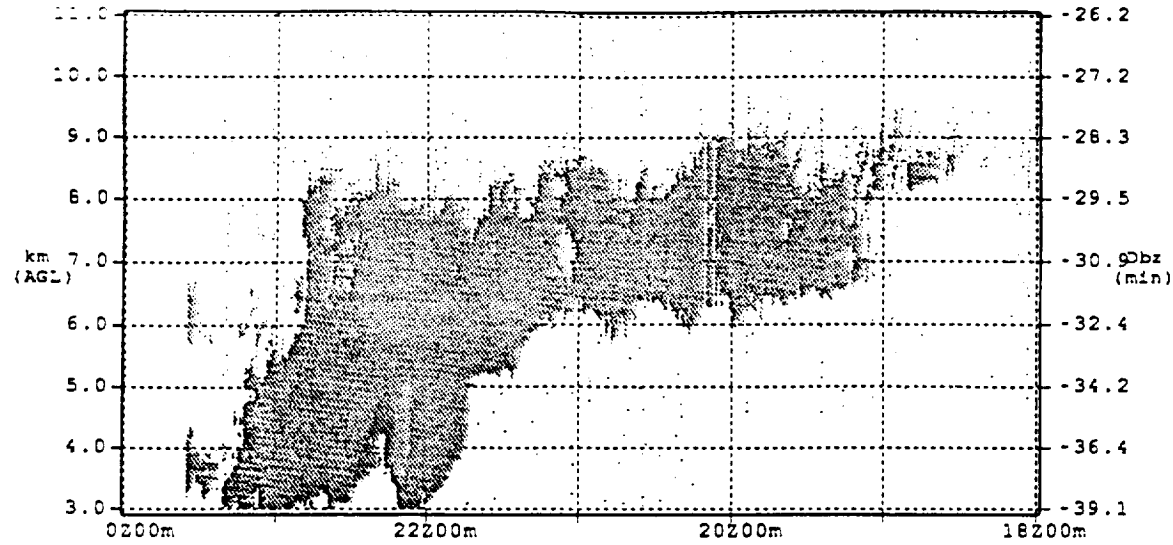

Fig. 3. Reflectivities (dbz) observed by the Pennsylvania State University 94 GHz cloud radar from 18 UTC 26 Nov 1991 to 00 UTC 27 Nov 1991. Time runs from right to left in the graph and the vertical scale is in kilometers

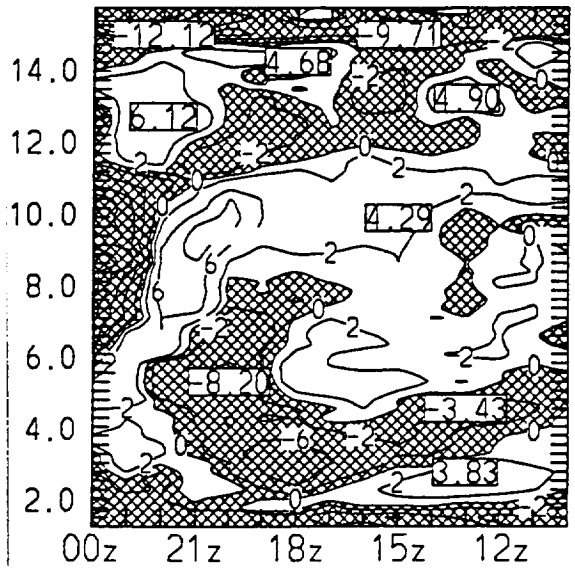

Fig. 4. Horizontal divergence calculated using the Q6 method and the profiler geometry of Fig. 1 with the Neodesha profiler (just north of Coffeyville) used as the central observation. Units are 10^{-5} s^{-1} and negative values are shaded. Time runs from right to left in the graph and the vertical axis is in kilometers.

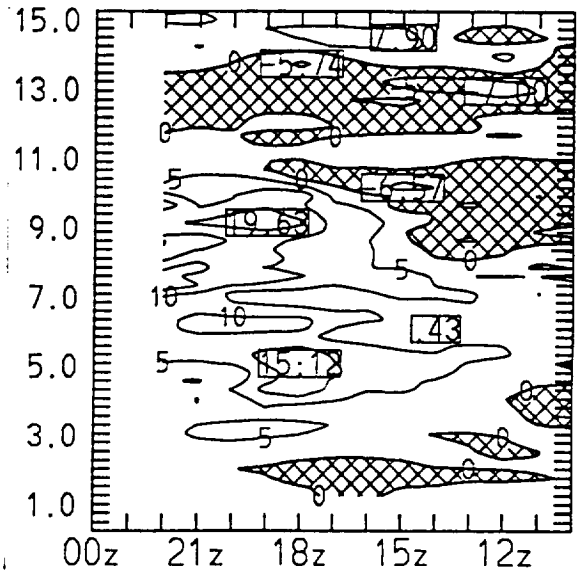

Fig. 5. Adiabatic vertical velocity (cm s^{-1}) calculated using horizontal winds from the Neodesha profiler and temperature gradients calculated using the CLASS radiosonde triangle created by the double square sites in Fig. 1. Plotting convention is as in Fig. 4.

the trough axis (Fig. 4) is much as would be expected: lower and middle tropospheric convergence coupled with upper tropospheric divergence. The appearance of the upper level cloud shield over the cloud radar is well correlated with the layer of divergence between 8.5 and 11 km and the onset of convergence below 8 km. Comparing the divergence pattern with the adiabatic vertical velocities (Fig. 5), a good degree of correlation can be seen. Before the onset of cloudiness, the upper tropospheric divergent layer between 8.5 and 11 km can be seen to drive upward motion from below and downward motion from above, qualitatively in line with mass continuity expectations. Upward motion is also resolved before and during the passage of the cloud band over the observational network. This pattern is, however rather noisy and the maximum

upward motion at 9 km between 18z and 20z is above the top of the cloud layer. The noisiness of the vertical velocities during the cloud event may well be due to a failure of the adiabatic assumption. Fig. 6, which shows the network observed vertical velocities, is highly correlated with the passage of the cloud band over the network and in line with the divergence pattern (see the extended discussion in Mace et al., 1992).

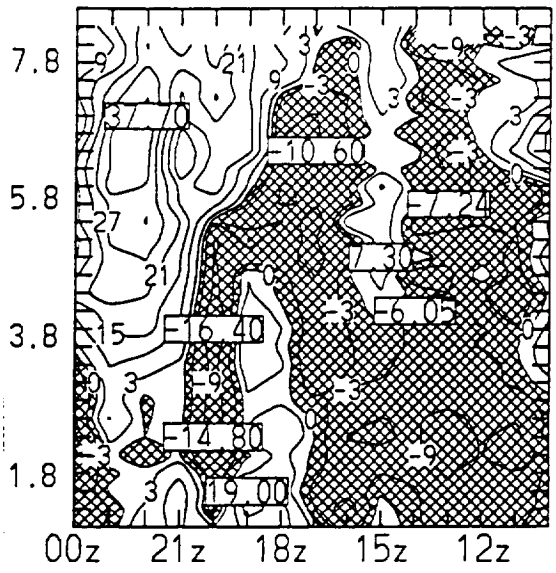

Fig. 6. Profiler observed vertical velocities in units of cm s^{-1}. These are triangle mean values calculated using the three profiler within the marked pentagon of profilers in Fig. 1. Plotting convention is as in Fig. 4.

Fig. 7 shows a plot of vapor pressure gradient vectors obtained from the radiosonde triangle shown in fig. 1. These vectors, which point up the water vapor pressure gradient, clearly delineate the passage of the cloud band. After 15z , the vectors above 3 km point westward, indicating that water vapor is increasing to the west (toward the advancing cloud band). As the cloud band passes over the network, the vectors tend to turn clockwise with time. The passage of the axis of the water vapor maximum at a given height is marked by a turning of the vectors from a westward component to an eastward component. Note that the axis of the vapor pressure maximum tends to be resolved at continuously lower levels. A rather remarkable degree of correlation can be seen in this pattern with the descent of cloud top observed by the cloud radar. Fig. 8, which shows the water vapor flux convergence at 4.0 and 6.5 km, indicates that horizontal advection of water vapor was the predominant mechanism by which water vapor was transported into the cloud region. At 6.5 km the flux divergence was negative, or convergent long before any cloud was observed over the radiosonde network. A maximum convergence was resolved at 21z at 6.5 km. At this time the axis of the water vapor gradient passed over the observational network. A divergent flux of water vapor was resolved by 23z, just after dissipation of cloud over the network was observed by the cloud radar. At 4 km, vertical advection of water vapor contributed much more than at 6 km. The flux of water vapor remained nearly zero or divergent until after 19z when the term became strongly convergent. Maximum reflectivities were observed just after the maximum flux convergence was diagnosed.

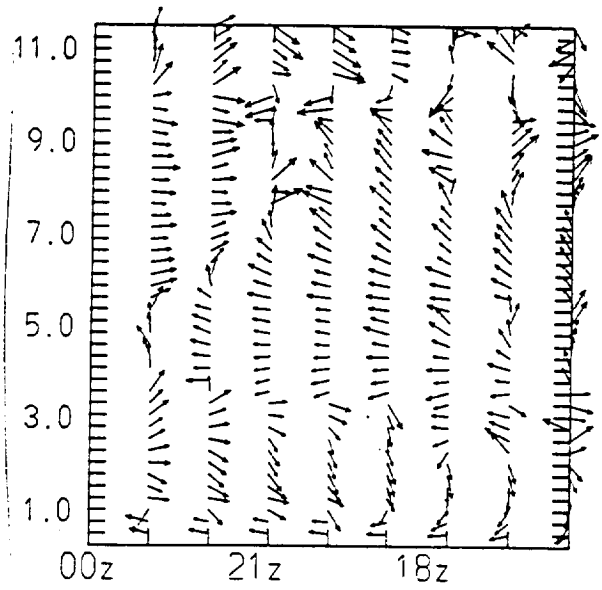

Fig. 7. Water vapor gradient vectors. The vectors point up the water vapor gradient or toward increasing values of water vapor. These values were calculated using the CLASS radiosonde sites shown in Fig. 1. Vectors are compass direction, time runs from right to left in the figure and the vertical axis is in kilometers.

4. SUMMARY

We have outlined methods which take full advantage of the number of wind profilers in the Kansas-Oklahoma region to generate kinematic quantities of the atmospheric flow. The method we have outlined

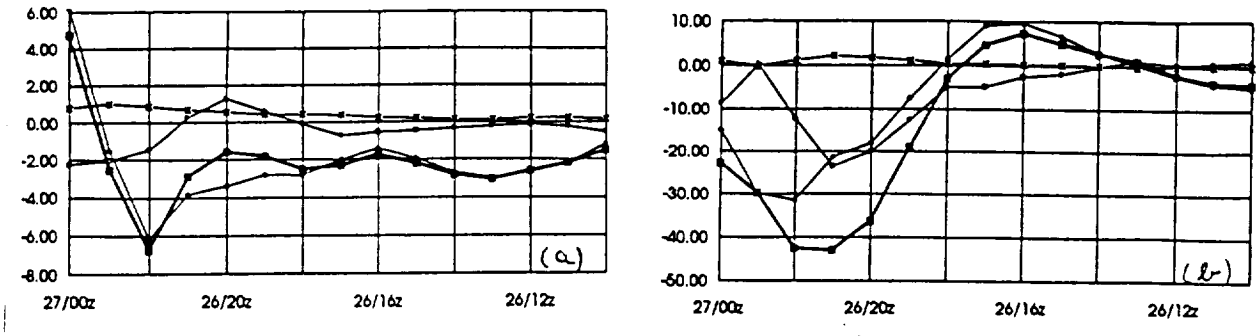

Fig. 8. Three dimensional water vapor flux convergence (mb hr^{-1}), $\nabla \cdot Ve$ plotted in the heavy line, the horizontal advection $V_h \cdot \nabla_h e$ plotted with a diamond, the vertical advection $w\,\partial e/\partial z$ plotted with an open circle and the divergent component $e(\nabla \cdot V)$ plotted with an asterisk. Units are in mb/hour. Time runs from right to left in the graphs. a: 6.5 kilometers. b: 4.0 kilometers

here is more accurate than previously published triangle methods since it considers the nonlinear components of the flow. This algorithm is currently being implemented operationally at the SGP CART site.

By combining the profiler kinematic quantities with radiosonde network derived quantities we have diagnosed the large scale dynamical forcing of a mesoscale cloud band. We find that the interaction of this forcing with the ambient water vapor field played a crucial role in the cloud system lifecycle.

Work is underway at the present time to rely more heavily on quantities derived from the wind profilers. Using thermal wind arguments, it can be shown that the adiabatic vertical velocities, thermal gradient information and geostrophic winds can be determined simultaneously from a network of wind profilers and a single vertical temperature profile provided by RASS or radiosonde. When applied to the FIRE Cirrus II using the radiosonde data collected at Coffeyville, an experiment long climatology of diagnostic quantities can be created. This information can then be used as model verification or as a statistical database.

Acknowledgments: This research benefitted greatly from many useful discussions with Dr Bruce Albrecht, Dr. Dennis Thomson and Mr. Mark Miller. Miss Laurie Bothell expertly helped in drafting the figures. This research was supported under NASA Grant NAG-1-1095 and DOE ARM Grant DE-FG02-90ER61071.

REFERENCES

Benjamin, S. G., 1989: An isentropic meso-alpha scale analysis system and its sensitivity to aircraft and surface observations. *Mon. Wea. Rev.*, 117, 1586-1605.

Holton, J. R., 1979: *An Introduction to Dynamic Meteorology*. Academic Press, 391 pp.

Mace, G. G., T. P. Ackerman, B. A. Albrecht, E. Clothieaux, 1992. A critical examination of methods used to calculate the kinematic properties of the atmospheric flow. Submitted to *Mon. Wea. Rev.*,

Peters, M. P., B. A. Albrecht, M. A. Miller, J. T. Treaster, 1992: Automated cloud profiling with a 94 GHz radar . Preprints, 11th International conference on Clouds and Precipitation, Montreal, 17-21 August, 1991, American Meteorological Society.

Zamora R.F., M.A. Shapiro, and C.A. Doswell III, 1987: The diagnosis of upper tropospheric divergence and ageostrophic wind using profiler wind observations.*Mon. Wea. Rev.*, 115, 871-884.